

Non-equilibrium phase transitions in hybrid Voronoi models of cell colonies

Mattia Miotto,¹ Giancarlo Ruocco,^{1,2} and Matteo Paoluzzi²

¹*Center for Life Nano & Neuro Science, Italian Institute of Technology, Viale Regina Elena 261, Rome, Italy.*

²*Department of Physics, Sapienza University of Rome, Piazzale Aldo Moro, Rome, Italy.*

Eukaryotic cells are characterized by a stiff nucleus whose effect in modeling the collective behavior of cell aggregates is usually underestimated. However, increasing experimental evidence links nuclear modifications with phenotypic transition, like the one between epithelial and mesenchymal states. In this work, we explore the effect of short-range repulsive forces in the non-equilibrium dynamics of the self-propelled Voronoi model. We show that the competition between steric repulsions (representing nuclear/cellular compressibility) and Vertex interactions (mimicking cell-cell adhesion/interaction and cytoskeleton organization) generate a variety of non-equilibrium phase transitions from Motility-Induced Phase Separation to mesenchymal-like phases up to disordered confluent configurations. Notably, we found that tuning the nucleus's effective size/compressibility provides an additional way to cross the boundary between the different possible phases in line with experimental observations.

I. INTRODUCTION

Biological tissues are collections of cells at high packing fractions. Each cell is a complex non-equilibrium machine; on top of that, cells are also deformable objects whose shape can fluctuate because of the interaction with the surrounding environment. Various models incorporate some of those minimal ingredients for capturing the collective behavior of cells in confluent monolayers [1–4]. Depending on the biological situation of interest, different coarse-graining descriptions of cells might be very effective. Those descriptions range from particle-based models [5–9], phase field models [10–16], Potts models [17–20], and Voronoi/Vertex models [21–30]. This is important for understanding biological processes during morphogenesis [31] or cancer invasion [32–34]. In its complexity, a single cell is characterized by different structures that are hierarchically arranged: in the spirit of coarse-graining only the leading degrees of freedom are necessary for describing cell collectives, most of the attempts in modeling the single cell neglect such a complexity. For instance, within phase fields and Voronoi-like models, cell shape fluctuations can be included as a leading ingredient necessary for modeling the cell aggregate more realistically. Such fluctuations have been found to act as a driving force for jamming/unjamming transition [35, 36]. In particular, elongated cells characterized by a high shape factor, i.e., the ratio between the typical cell perimeter divided by the square root of the cell area, tend to aggregate into a liquid phase where cells continuously rearrange [22]. Highly symmetric cells, characterized by a smaller shape factor, undergo a rigidity transition similar to the jamming phase or, in some cases, a glass-like transition [23, 37]. Many experimental studies provide evidence for the importance of non-equilibrium glass-like or jamming-like transition in confluent monolayers [35, 36, 38, 39]. Indeed, development, wound repair, and cancer metastasis are fundamental biological processes in which epithelial cells, typically non-migratory, can become highly mobile and rearrange over time and length scales much larger than the typical time

and length scales of the single cell. From a biological point of view, the transition from a sedentary to a migratory state in epithelial layers was thought to rely on EMT or partial EMT (pEMT) in many contexts. During EMT/pEMT, cells lose their apicobasal polarity and epithelial markers, while acquiring front-to-back polarity and mesenchymal markers, allowing them to detach from neighboring cells and the surrounding matrix, adopting a migratory behavior. The unjamming transition has been identified as a distinct migratory mechanism where collective epithelial migration may take place without EMT [40].

While cells can change their shape, allowing for adapting to growth in different conditions and moving across barriers [41], the presence of a stiff nucleus poses limits to their degree of deformability. In this framework, arises the question of what the effect of such stiff nucleus on cell collective behavior is (see for instance the reviews [42, 43]). Registering migration speed and cell/nucleus shapes, Wolf *et al.* [44], identified deformability of the nucleus as one of the first-order rate-limiting physicochemical determinants of cell migration. Grosser *et al.* [45] compared spheroids of cancerous and non-cancerous cell lines via bulk experiments and/or single live-cell tracking, finding that cancerous cells populations are fluidized by active cells moving through the tissue with the degree of tissue fluidity correlating with elongated cell and nucleus shapes. They speculate that individual cell and nucleus shape may serve as a marker for metastatic potential. Despite increasing evidence of the mechanical importance of the cell nucleus, models explicitly accounting for its effect are still rare [46].

What is the effect of combining a stiff nucleus with a deformable shape in collective cell behaviors remains an open question. Here, we introduce a hybrid Voronoi model that takes into account short-range excluded volume forces mimicking the presence of the stiff cell nucleus. Our hybrid Voronoi model allows us to describe cells in both mesenchymal and epithelial phases. Indeed, by varying the relative strength between Vertex and excluded volume forces we interpolate from a pure particle-based model to a confluent model. Note that

our approach counts a few control parameters for controlling different ingredients as typical shape elongation, cell motility, and nuclei stiffness. In contrast, other approaches require the fine-tuning of many parameters and is quite expensive from the numerical point of view [1]. In the following, after introducing the model, we show that the system undergoes several non-equilibrium phase transitions from the so-called Motility-Induced Phase Separation (MIPS) [47], to standard active liquid, to Voronoi (confluent) liquid, and disordered solid by tuning the strength of the Vertex interaction. Next, we change the packing fraction of the system showing that this brings a reach phase diagram where cells can arrange in Gas-like or Phase-separates without attractive forces at low packing fraction (as in the case of Mesenchymal cells). By increasing the strength of Voronoi the system becomes confluent. However, the structural property of the monolayer changes dramatically with the packing fraction.

II. HYBRID VORONOI MODEL

We consider a system composed of N cells confined into a square box of side $L = \sqrt{N}$ with periodic boundary conditions. We indicate with \underline{r}^i the position of the i -th cell center (with $i = 1, \dots, N$) whose equation of motion reads

$$\dot{\underline{r}}^i = v_0^i \hat{e}_i + \mu \underline{E}_i \quad (1)$$

where \underline{E}_i is the total force acting on the cell, μ the mobility, and v_0^i the modulus of the self-propulsion velocity whose direction in 2D is given by the versor \hat{e}_i that, in 2D, is parameterized by the angle θ_i , i.e., $\hat{e}_i = (\cos \theta_i, \sin \theta_i)$. In the following, the modulus of the self-propulsion velocity is the same for each cell $v_0^i = v_0$.

As a model for the active motion, we consider Active Brownian dynamics in which the orientation of the self-propulsion θ_i follows a standard Langevin equation of the form $\dot{\theta}_i = \eta_i$, with $\langle \eta_i \rangle = 0$ and $\langle \eta_i(t) \eta_j(s) \rangle = \frac{2}{\tau} \delta_{ij} \delta(t-s)$. Here, we introduce the persistence time of the active motion, τ that is the inverse of the rotational diffusivity coefficient D_r .

Finally, we consider the case where the total mechanical force acting on each cell splits into two contributions. The first term regulates cell fluctuations, and the second one represents nucleus incompressibility. We thus write \underline{E}_i as follows

$$\underline{E}_i = \nabla_{\underline{r}_i} [\epsilon E_v + (1 - \epsilon) \Phi] \quad (2)$$

where ϵ is a parameter tuning the relative intensities of geometrical (E_v) and nuclear repulsion (Φ) energies. Note that for $\epsilon = 0$ one recovers the active particle model while for $\epsilon = 1$ the system behaves as the standard Voronoi model. In Fig. (1)a-b we depict the relevant features of the model. In particular, the term $E_v = \frac{1}{2} \sum_i^N E_v^i$ is the geometrical energetic contribution

given by the Vertex energy:

$$E_v^i = K_p(p_i - p_0)^2 + K_a(A_i - A_0)^2 \quad (3)$$

in which p_i and A_i represent the perimeter and area of cell i , respectively; K_p , K_a are constants depending on the specific cell type. The area modulus K_a determines how resistant a cell is to deviations from its preferred area. It penalizes deviations of the actual area of the cell from its target area A_0 . The latter reflects the size that cells tend to maintain due to internal forces such as pressure, growth constraints, or packing density. Similarly, K_p is the perimeter elasticity constant or perimeter modulus, which controls how resistant a cell is to changes in its perimeter with respect to its preferred perimeter p_0 . Analogous to the preferred area A_0 , the target perimeter reflects the cell's preferred shape in terms of its perimeter and typically accounts for the contractility of the actomyosin network at the cell boundary. Without losing generality, one can set K_p , K_a , and A_0 to one, and keep p_0 as control parameters.

It is now well established that a system subject only to vertex energy displays a phase transition between a solid and liquid-like behavior for $p_0 \sim 3.81$ (see for instance Bi *et al.* [23]). In the present work, we consider another key feature of cell architecture, i.e. the steric hindrance exerted by cell nuclei, whose stiffness ultimately limits the compressibility of cell layers. To this aim, we inserted a repulsive interaction between cell nuclei given by $\Phi = \sum_{i < j} \phi(r_{ij})$ and :

$$\phi(r) = \left(\frac{\sigma_0}{r} \right)^{12} \quad (4)$$

where σ_0 gives an effective size for the cell nucleus. Our proposed model combines repulsive interactions, given by the excluded volume effect due to nuclei stiffness to the Vertex energy term which promotes a spatial configuration of the system described by a Voronoi tessellation. The vertex energy considers mechanical interactions due to cell shape fluctuations in a regime where each cell is surrounded by neighbor cells. This is a typical scenario of a confluent tissue. Note that within Voronoi models any fluctuation (weakly) preserving cell area is allowed. Our model allows us to explore the tradeoff between the behavior produced by highly deformable cells where excluded volume is dominated by the presence of the nucleus and the regime in which the whole cell has a relevant stiffness.

III. RESULTS AND DISCUSSIONS

Our model allows one to study systematically the interplay between motility, excluded volume, and geometrical interactions. It is well established that self-propelled agents undergo a non-equilibrium phase separation without attractive forces called MIPS [47]. MIPS is possible because of the interplay between excluded volume forces

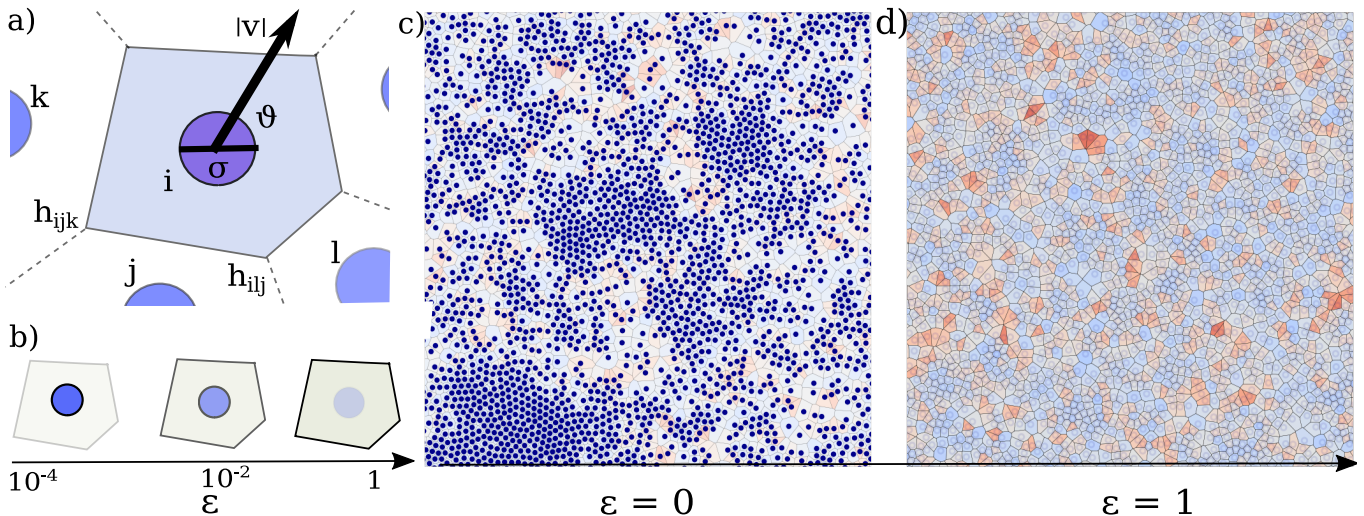


FIG. 1: **Model of cell colony.** **a)** Schematic representation of a cell: effective cell surface is given by a Voronoi tessellation of the 2D plane, while the nucleus is rendered via the repulsive interaction and has an effective diameter of σ . Self-propulsion is described by a velocity vector of constant modulus and instantaneous direction. **b)** Schematic representation of the trade-off between the repulsive potential energy and the Voronoi interaction acting among cell nuclei. The relative intensity of the two terms is modulated by the ϵ parameter introduced in Eq. 2. **c)** Snapshot of a cellular dynamics simulation in the pure repulsive regime with a long persistence time. Cell nuclei are represented as blue circles. The corresponding Voronoi tessellation is shown on the background with shaded colors. **d)** Snapshot of a cellular dynamics simulation in the pure Voronoi regime. Cell colors range from dark blue to dark red as the cell shape factor increases.

and persistent motion: the former triggers feedback between local velocity and local density that eventually makes the homogeneous density profile unstable driving the system into a phase separation. On the other hand shape fluctuations and motility can change the morphology of a confluent driving another non-equilibrium phase transition between fluid and disordered solid [23]. We now explore how the combination of these effects changes the structural and dynamical properties of cell collectives. To do so, we first study the competition between excluded volume and geometrical forces in a regime where the active particles are in the MIPS phase. After that, we first study the structural property of the active fluid approaching the disordered phase, then we tune the density of the system by changing the typical nucleus size.

A. Competition between excluded volume repulsion and geometrical forces

Ultimately, the two potential energy terms when considered alone (in the presence of active motion) promote spatially homogeneous configurations of non-regular cells for the Vertex interaction, while homogeneous configurations of regular shape polygons are observed when considering only short-range repulsion (see Figure 1c-d for a representation).

To explore the interplay between the two terms, we considered a homogeneous population of cells with a nucleus effective radius of $\sigma_0 = 0.5$, self-propulsion velocity of $v_0 = 0.5$ and shape index, $s_0 = 3.2$, and studied

the non-equilibrium steady state behavior of the system upon varying the relative strength of the two potential terms via tuning the ϵ parameter. As one can see from the trajectories of the cell centers displayed in Figure 2a, the pure Voronoi regime is associated with a solid-like motion of the cells, whose centers oscillate around quasi-fixed positions. This is following previous observations on Voronoi models with the same parameter set [23]. Increasing the contribution of the nuclear repulsion, the system behaves more like a fluid, with trajectories having higher mean square displacements. In particular, the average difference between cell's initial and final position presents a sigmoidal trend as a function of ϵ associated with a solid-to-fluid phase transition of the system. Moreover, the critical ϵ increases as a function of the cell shape factor (orange curve in Figure 2b) and reaches the limiting value of 1 for $s_0 \sim 3.8$, as one would expect since the pure Voronoi model is known to exhibit a disordered solid to fluid transition upon varying the cell shape index. Next, we analyzed the behavior of the cell population in the fluid region of the phase diagram. In the pure repulsive regime ($\epsilon = 0$), cells act like homogeneous active particles of effective size σ_0 . Such systems are known to exhibit MIPS as a function of the persistence time of the active motion, τ . The transition between a homogeneous gas phase to a mixture of a low-density fluid-like phase and an ordered crystal-like phase as a function of τ can be quantitatively measured by looking at the static structure factor of the system, $S_s(q)$, at low q vectors. In particular, Figure 2c shows the behavior of the static structure factor in log-log scale for three different values

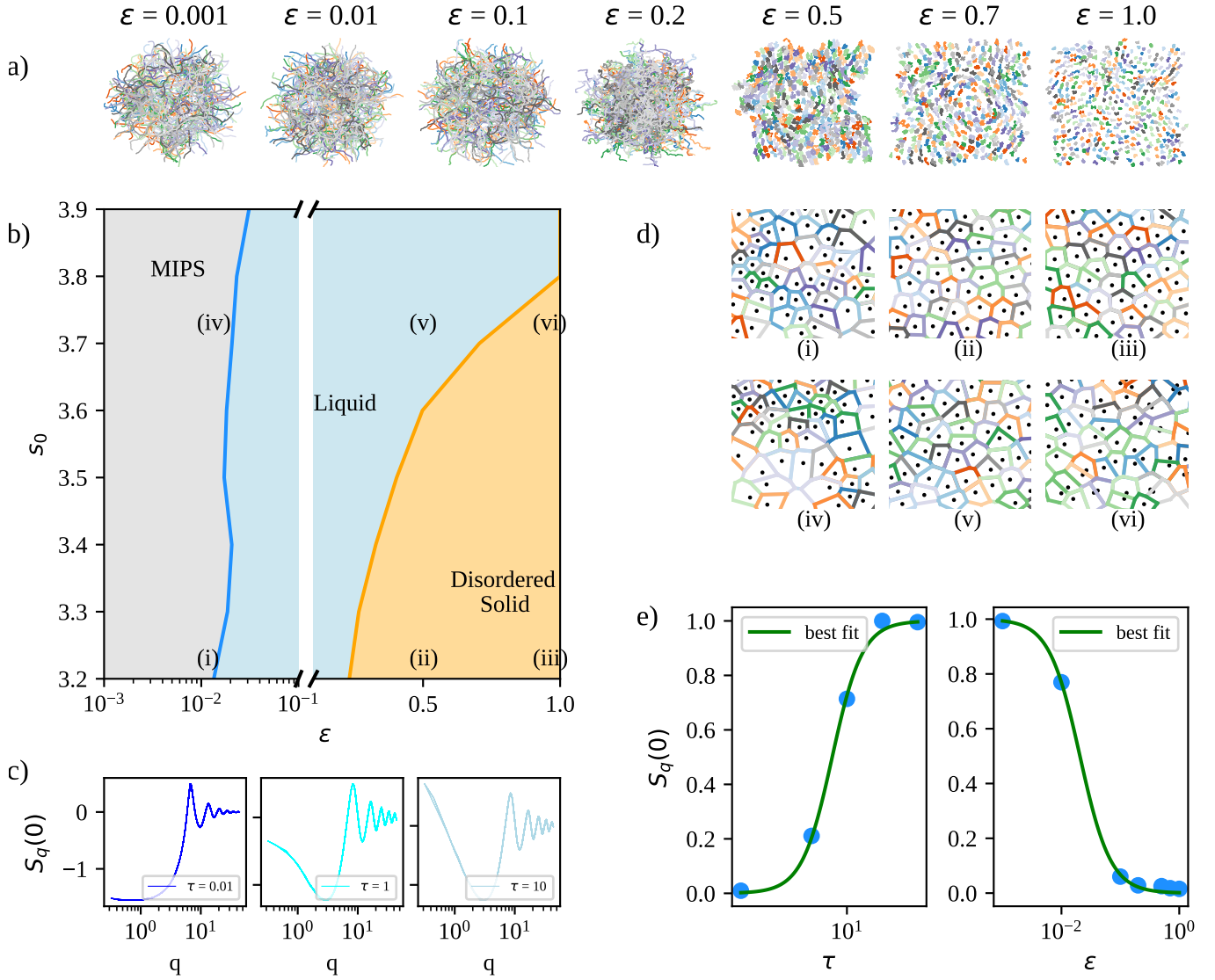


FIG. 2: Competition between nuclear short-range repulsion and geometrical forces. (a) Representative trajectories by increasing the strength of the geometrical force. (b) Phase diagram of the behavior of the cell population as a function of the intrinsic shape factor, $s_0 = p_0/\sqrt{A_0}$ and the relative strength of the geometrical force vs the nuclear repulsive ones. (c) Static structure factor of a cell population for different values of the persistence time, τ in the limit of pure nuclear repulsion ($\epsilon = 0$). (d) Voronoi tessellation of a set of representative snapshots of the population in the stationary regime for different choices of ϵ and s_0 , marked in the phase diagram reported in panel b). (e) Normalized structure factor at long distances ($q = 0$) as a function of the persistence time in the pure nuclear repulsion regime (left) and as a function of the relative strength of the geometrical force for cell population having persistence time of 10^3 (right). Blue dots mark the value extracted from simulations, while the green line corresponds to the best-fit solution of the sigmoidal function, $y/y_{max} = 1/(1 + e^{-x/x_0})$. Flex points mark the boundaries of the MIPS.

of the persistence time. As one can see the static structure factor at long distances increases as the persistence time of the active motion increases in a sigmoidal fashion with critical $\tau \sim 10$ (see Figure 2e). Looking at the low q value of the static structure factor as a function of the relative strength of the potential terms and of the cell shape factor, we found that the system presents a phase transition between MIPS and standard active liquid for

values of $\epsilon \sim 0.02$ as shown by the best fit in Figure 2e and the blue line in Figure 2b.

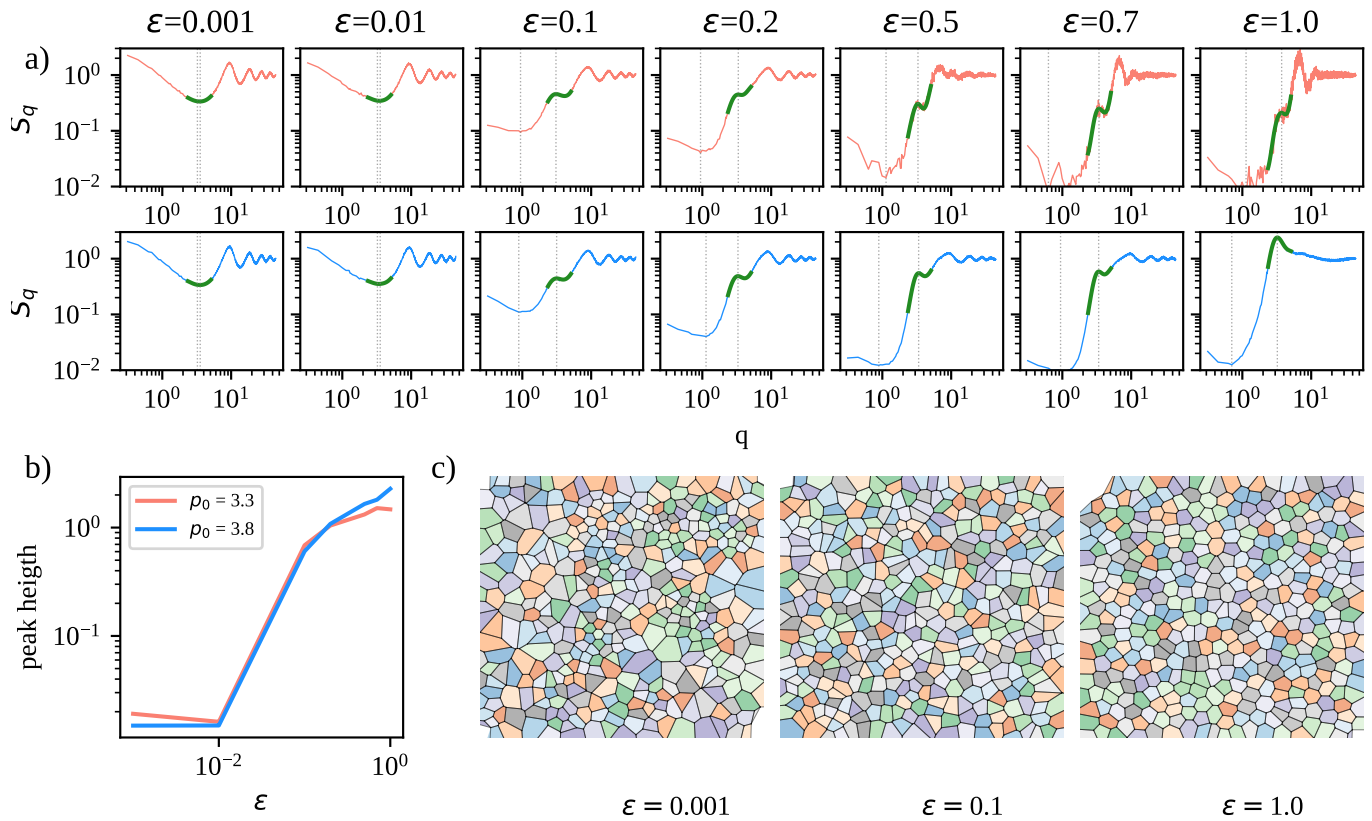


FIG. 3: **From standard to confluent active fluid.** a) Static structure factor as a function of the relative strength between repulsive and geometrical forces, ϵ , for two choices of the cell-intrinsic shape factor, s_0 . The top row (respectively bottom) reports results for $s_0 = 3.3$ (resp. $s_0 = 3.8$). Green line makes the region corresponding to the expected Voronoi peak. b) Difference between the maximum and minimum values of the static structure factor in the region of the Voronoi peak highlighted in panel a) as a function of the relative strength between repulsive and geometrical forces. c) Voronoi tessellation of snapshots taken from the stationary phase of a cell dynamics with three different values of the ϵ parameter.

B. Cell-cell force intensity regulates standard to confluent active fluid.

Further analyzing the behavior of the static structure factor, we observed that besides the trend at $q = 0$, carrying information on MIPS, and the oscillating trend at high q , characteristic of fluids, the curves present a peculiar behavior at intermediate values of $q \sim 3$, where a peak start appearing as the values of ϵ becomes higher than the critical one separating the MIPS phase from the liquid one (see green shaded regions in Figure 3a). Specifically, measuring the height of the peak as the difference between the static structure factor at the maximum of the peak and its value in the nearer minimum found at lower values of q (dotted vertical lines in Figure 3a), one can see that the peak intensity increases by tuning the strength of the Vertex interaction, as shown in panel b) of Figure 3. The progressive dominance of this peak (which is not dependent on the cell shape factor), marks the passage from a standard active liquid to a Voronoi (confluent) liquid. Cells develop different short-range structures depending on the strength of Voronoi (see also the representative snapshots in Figure 3c).

C. Nucleus size as a driver for the Epithelial-to-Mesenchymal transition in cell colonies

In the Voronoi model the packing fraction φ is set to unit: this is because one usually considers the Voronoi tessellation generated by N centers in a square box of side \sqrt{N} . The ingredient of the cell nucleus introduces another typical length, i.e., the nucleus size σ_0 , that allows us to vary φ . Active particle systems are known to undergo different phase transitions depending on the ratio between the volume occupied by the particles, i.e. the excluded volume, and the total volume. The more φ approaches its maximum value ($\varphi = 1$), the more cells dispose of in an ordered hexatic phase, while on the other extreme, for low packing fractions, the system assumes the behavior of a particle gas (see Figure 4a). In between, motility-induced phase separation is reported as a function of the persistence time and cell effective radius. To assess the effect of cell nuclei on the colony behavior, we explore the phase diagram as a function of nuclear size, σ_0 and the relative strength of the Vertex vs nuclear repulsive potentials, ϵ while maintaining both cell self-propulsion velocity, persistence time and system

total volume fixed.

Changing the cell nucleus size, i.e. the packing fraction of the system, brings a rich phase diagram where the cell population can arrange in Gas-like or Phase-separates without attractive forces at low packing fraction (a behavior typical of mesenchymal cells), as one can see from Figure 4b1 and c1 where we reported the diagrams obtained for a persistence time of 50 and target perimeters of $p_0 = 3.2$ and 3.9, respectively. By increasing the strength of Voronoi, the system becomes confluent. However, the structural property of the monolayer changes dramatically with both the packing fraction and target perimeter displaying both disordered to ordered solid transitions and confluent fluid to disordered solid ones. The latter are phases typically associated with epithelial cells. Indeed, by inspecting the typical configurations observed in the different region of the phase diagrams, we can distinguish both the aggregated clusters of cells in the MIPS region (see Figure 4b2-(i) and c2-(ii)) and the hexagonal disposition of the cells that indicate the presence of a crystal-like behavior of the 2D cell layer (Figure 4b2-(iii) and c2-(i)). The observed behaviors are further confirmed by looking at the static structure factors (see Figure 4b3-c3). Finally, analyzing the region of the diagram characterized by low values of both ϵ and σ_0 , we found a transition between a gas-like to a liquid-like phase upon increasing the relative ratio between cell-cell adhesion strength and nuclear size as shown in both the configurations of Figure 4b2-(ii) and c2-(iii), and quantified by the shape of the respective structure factors.

IV. CONCLUSIONS

We proposed the hybrid-Voronoi model able to account for the nuclear stiffness in influencing the collective behavior of biological tissues, building on key models that capture the mechanical and dynamic properties of cellular structures. Tissue models are governed by specific degrees of freedom, notably shape fluctuations, which play a critical role in driving the transition between jamming and unjamming states, and cellular motility, which induces glassy dynamics. However, cells are not fully deformable; they contain a stiff nucleus that limits their malleability, raising the question of how this nuclear stiffness impacts collective tissue behavior.

Previous research has shown that nuclear rigidity can significantly affect tissue dynamics and morphogenesis, yet integrating this aspect into computational models has often proven challenging. To address this, our model utilizes a hybrid Voronoi approach, enabling the simulation of cells in both mesenchymal and epithelial phases by adjusting the strength of the vertex energy. This approach provides a smooth transition from particle-based to confluent modeling, effectively capturing cellular phase behavior without the computational cost and extensive parameter tuning required by phase-field models.

The hybrid Voronoi model requires only minimal pa-

rameterization—namely, the nuclear stiffness, shape parameter, and motility parameter—allowing for efficient yet realistic simulations of collective cell dynamics. This streamlined parameter set provides a powerful tool for exploring how variations in nuclear stiffness influence tissue behavior, offering valuable insights into the mechanics underlying tissue organization and transitions.

Using the relative strength between excluded volume forces and Voronoi forces, we observe that Voronoi interactions promote uniform configurations so that MIPS reverse into a homogeneous active fluid phase and eventually to disordered solids. In other words, as a general result, we obtain that surface interactions such as the ones generated by the Vertex configurational tend to destroy any kind of cluster formation: this is a critical feature that might be tested against experiments.

On the other hand, moving from fluid to disordered solid, we observe a sort of liquid-liquid smooth crossover from an active fluid phase to a Voronoi fluid phase. We have documented this behavior through the low- q behavior of the static structure factor $S(q)$ that signals a change in the local structures of the active fluid by varying ϵ . Changing the packing fraction we obtained a phase diagram that counts several phases: the MIPS phase, a Liquid phase, a crystallization region, and a disordered solid state. The small- ϵ regime of the phase diagram is consistent with the literature of active matter [8, 48]. From a biological viewpoint, our results suggest modulation of nuclear size/stiffness may work as an additional layer of control to tune the mechanical properties of cell colonies besides the known regulation of the apico-basal polarity and cell-cell adhesion. Notably, our findings corroborate the recent observations on the effects of nuclear shape/size in modifying the fluidity of cancer cell organoids [45]. As a future direction, it might interesting to account for alignment interaction that has been shown to play a crucial role in cell rearrangements [38, 49].

V. METHODS

A. Forces calculation

Here, we derived exact analytical expressions for the forces acting on each cell center with respect to the energy defined by Eq. 2.

In particular, we need to explicit the geometrical and repulsion terms, i.e $\nabla_{\mathbf{r}_i} E_v$ and $\nabla_{\mathbf{r}_i} \Phi$, respectively.

1. Geometrical force

The geometrical force acting on the nucleus center of cell i is obtained deriving the total Vertex energy:

$$\vec{F}_v^i = -\frac{dE_v}{d\vec{r}_i} = -\frac{dE_v^i}{d\vec{r}_i} - \sum_{j \in N(i)} \frac{dE_v^j}{d\vec{r}_i} \quad (5)$$

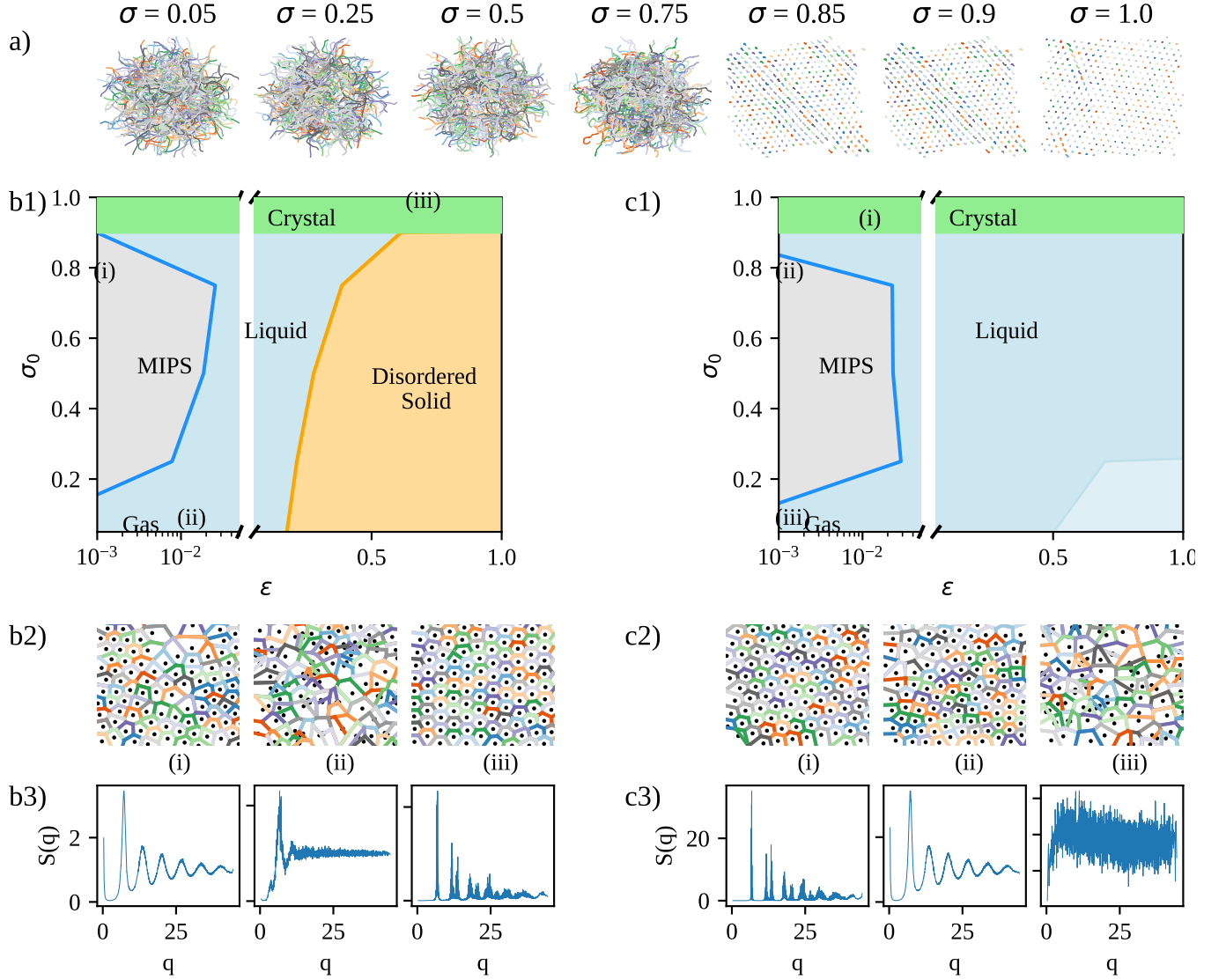


FIG. 4: **Nucleus size as a driver for the Epithelial-to-Mesenchymal transition in cell colonies.** **a)** Representative trajectories by increasing the nuclei size in the presence of weak geometrical forces. **b1)** Phase diagram of the behavior of cell colonies as a function of the relative weight of repulsion/geometrical forces, ϵ and of nuclei size, σ_0 . Lines mark the borders between the different observed phases. Cells are characterized by an intrinsic shape factor of 3.3. **b2)** Voronoi tessellation of three snapshots taken from the stationary dynamics of a cell population with different values of ϵ and σ_0 , as shown in panel b1). **b3)** Static structure factor measured in population on cells characterized by the three sets of parameters from with snapshots in panel b2) are drawn. **c1-3)** Same as in panels b1-3) but considering cells with an intrinsic shape factor of 3.8.

where $N(i)$ represents the near neighbours of cell i .

The general term $\frac{dE_i^\alpha}{dr_i^\alpha}$, i.e. the component α of the variation of the energy of cell i when moving the center of cell j , can be written using the following chain rule:

$$\frac{dE_i^\alpha}{dr_j^\beta} = \sum_\nu \frac{dE_i^\alpha}{dh_{ijk}^\nu} \frac{dh_{ijk}^\nu}{dr_j^\beta} + \sum_\nu \frac{dE_i^\alpha}{dh_{ijl}^\nu} \frac{dh_{ijl}^\nu}{dr_j^\beta} = \quad (6)$$

where \vec{h}_{ijk} and \vec{h}_{ijl} are the two shared vertexes between cells i and j .

We have to evaluate the change in energy of a cell upon moving one of its vertexes and the variation in the position of a vertex when moving a cell center.

The former is given by:

$$\frac{dE_i^\alpha}{dh_{ijk}^\nu} = 2K_p(p_i - p_0) \frac{dp_i}{dh_{ijk}^\nu} + 2K_A(A_i - A_0) \frac{dA_i}{dh_{ijk}^\nu} \quad (7)$$

with

$$\frac{dp_i}{dh_{ijk}^\nu} = -(\hat{t}_{kj} + \hat{t}_{ki}) \quad (8)$$

and $\vec{t}_{kj} = \vec{h}_{ijk} - \vec{h}_{kjl}$ and $\vec{t}_{ki} = \vec{h}_{ijk} - \vec{h}_{lik}$, i.e. the oriented vector having the direction of the edge between the moving vertex (dh_{ijk}) and the two vertexes that share a cell with it. Note that the directions of the defined vectors are going from the moving vertex toward the other(s).

Similarly, the variation of the area upon moving the vertex is given by:

$$\frac{dA_i}{dh_{ijk}^\nu} = \frac{1}{2}(l_{ij}\hat{n}_{ij} + l_{ik}\hat{n}_{ik}) \quad (9)$$

where l is the length of a given \vec{t} and \hat{n} is the unit vector pointing outwardly normal to the cell edge.

To obtain an expression for the second term, $\frac{d\vec{h}_{ijk}}{d\vec{r}_j}$, we start from the relation that identifies the vertex shared between the cells, i , j , and k :

$$\vec{h}_{ijk} = A\vec{r}_i + B\vec{r}_j + \Gamma\vec{r}_k \quad (10)$$

with the coefficients given by:

$$A = \frac{\|\vec{r}_j - \vec{r}_k\|^2 (\vec{r}_i - \vec{r}_j) \cdot (\vec{r}_i - \vec{r}_k)}{D} = \frac{\|\vec{r}_{jk}\|^2}{D} \vec{r}_{ij} \cdot \vec{r}_{ik} \quad (11)$$

$$B = \frac{\|\vec{r}_{ik}\|^2}{D} \vec{r}_{ji} \cdot \vec{r}_{jk} \quad (12)$$

$$\Gamma = \frac{\|\vec{r}_{ij}\|^2}{D} \vec{r}_{ki} \cdot \vec{r}_{kj} \quad (13)$$

and

$$D = 2\|\vec{r}_{ij} \times \vec{r}_{jk}\|^2 = 2(r_{ij}^x r_{jk}^y - r_{ij}^y r_{jk}^x)^2 \quad (14)$$

(Note that we adopted the definition $\vec{r}_{ij} = \vec{r}_i - \vec{r}_j$)
So we have that:

$$\frac{\partial \vec{h}_{ijk}}{\partial \vec{r}_j} = \frac{\partial A}{\partial \vec{r}_j} \vec{r}_i + \frac{\partial B}{\partial \vec{r}_j} \vec{r}_j + \frac{\partial \Gamma}{\partial \vec{r}_j} \vec{r}_k + A \frac{\partial \vec{r}_i}{\partial \vec{r}_j} \quad (15)$$

and

$$\frac{\partial A}{\partial r_j^m} = \frac{1}{D} [\|\vec{r}_j - \vec{r}_k\|^2 (r_i^m - r_k^m + r_i^m - r_j^m)] - \frac{1}{D} A \frac{\partial D}{\partial r_i^m} \quad (16)$$

from which one can obtain:

$$\frac{\partial(DA)}{\partial r_i^m} = D \frac{\partial A}{\partial r_i^m} + A \frac{\partial D}{\partial r_i^m} = \|\vec{r}_{jk}\|^2 (r_{ik}^m + r_{ij}^m) \quad (17)$$

Similarly, we have that

$$\frac{\partial(DB)}{\partial r_i^m} = 2r_{ik}^m (\vec{r}_{ji} \cdot \vec{r}_{jk}) - \|\vec{r}_{ik}\|^2 r_{jk}^m \quad (18)$$

$$\frac{\partial(D\Gamma)}{\partial r_i^m} = 2r_{ij}^m (\vec{r}_{ki} \cdot \vec{r}_{kj}) - \|\vec{r}_{ij}\|^2 r_{kj}^m \quad (19)$$

$$\frac{\partial D}{\partial r_i^m} = 4 \left(r_{ij}^x r_{jk}^y - r_{ij}^y r_{jk}^x \right) \left[\delta_{mx} r_{jk}^y - \delta_{my} r_{jk}^x \right] \quad (20)$$

Finally, plugging all together we get:

$$\begin{aligned} \frac{\partial h_{ijk}^l}{\partial r_i^m} &= \frac{1}{D} \left(\frac{\partial(DA)}{\partial r_i^m} - A \frac{\partial D}{\partial r_i^m} \right) r_i^l + \\ &+ \frac{1}{D} \left(\frac{\partial(DB)}{\partial r_i^m} - B \frac{\partial D}{\partial r_i^m} \right) r_j^l + \\ &+ \frac{1}{D} \left(\frac{\partial(D\Gamma)}{\partial r_i^m} - \Gamma \frac{\partial D}{\partial r_i^m} \right) r_k^l + A \delta_{lm} \end{aligned} \quad (21)$$

2. Repulsive force

The repulsive force acting on the nucleus center of cell i is obtained by deriving the total repulsive energy

$$\vec{F}_r^i = -\frac{d\phi_r}{d\vec{r}_i} = \sum_{j \in N(i)} \frac{d\phi_r^j}{d\vec{r}_i} \quad (22)$$

and

$$\frac{d\Phi_r^j}{dr_i^\alpha} = -12 \left(\frac{\sigma_0^{12}}{r_{ij}^{13}} \right) \frac{(r_i^\alpha - r_j^\alpha)}{r_{ij}} \quad (23)$$

B. Observables

As order parameters describing the global properties of the system, we compute (i) the average long-time displacement of the cell nuclei $\langle \Delta \rangle$, where $\Delta_i = \sqrt{\sum_j^3 (x_j^i(t^*) - x_j^i(0))^2}$ and (ii) the static structure factor at small q , $S_q(q \rightarrow 0)$.

C. Simulation details

To perform the dynamics, we followed the same procedure used for MD simulations of molecules/particle systems: we first generate a system with a nucleus in random positions inside a squared box of edge $L = \sqrt{(N)}$ with periodic boundary conditions (to obtain them with replicate the system in every direction). Next, each simulation has been carried on for a total time of 10^4 , integrating equations of motions with a time step of 10^{-3} .

Data Availability

The data that support the findings of this study are available from the corresponding author upon reasonable request.

Code Availability

All codes used to produce the findings of this study are available from the corresponding author upon request.

Author contributions statement

All authors analyzed results, wrote and revised the paper.

Competing Interests

The authors declare no competing interests.

Acknowledgements

This research was partially funded by grants from ERC-2019-Synergy Grant (ASTRA, n. 855923); EIC-2022-PathfinderOpen (ivBM-4PAP, n. 101098989); Project ‘National Center for Gene Therapy and Drugs based on RNA Technology’ (CN00000041) financed by NextGeneration EU PNRR MUR—M4C2—Action 1.4—Call ‘Potenziamento strutture di ricerca e creazione di campioni nazionali di R&S’ (CUP J33C22001130001).

-
- [1] Ricard Alert and Xavier Trepap. Physical models of collective cell migration. *Annual Review of Condensed Matter Physics*, 11(1):77–101, 2020.
- [2] Xavier Trepap and Erik Sahai. Mesoscale physical principles of collective cell organization. *Nature Physics*, 14(7):671–682, 2018.
- [3] Brian A Camley and Wouter-Jan Rappel. Physical models of collective cell motility: from cell to tissue. *Journal of physics D: Applied physics*, 50(11):113002, 2017.
- [4] Daniel L Barton, Silke Henkes, Cornelis J Weijer, and Rastko Sknepnek. Active vertex model for cell-resolution description of epithelial tissue mechanics. *PLoS computational biology*, 13(6):e1005569, 2017.
- [5] Bart Smeets, Ricard Alert, Jir? Pesek, Ignacio Pagonabarraga, Herman Ramon, and Romaric Vincent. Emergent structures and dynamics of cell colonies by contact inhibition of locomotion. *Proceedings of the National Academy of Sciences*, 113(51):14621–14626, 2016.
- [6] Silke Henkes, Kaja Kostanjevec, J Martin Collinson, Rastko Sknepnek, and Eric Bertin. Dense active matter model of motion patterns in confluent cell monolayers. *Nature communications*, 11(1):1–9, 2020.
- [7] Fabio Giavazzi, Chiara Malinverno, Salvatore Corallino, Francesco Ginelli, Giorgio Scita, and Roberto Cerbino. Giant fluctuations and structural effects in a flocking epithelium. *Journal of Physics D: Applied Physics*, 50(38):384003, 2017.
- [8] Matteo Paoluzzi, Demian Levis, and Ignacio Pagonabarraga. From motility-induced phase-separation to glassiness in dense active matter. *Communications Physics*, 5(1), May 2022.
- [9] Matteo Paoluzzi, Demian Levis, and Ignacio Pagonabarraga. From flocking to glassiness in dense disordered polar active matter. *Communications Physics*, 7(1):57, 2024.
- [10] Danying Shao, Wouter-Jan Rappel, and Herbert Levine. Computational model for cell morphodynamics. *Phys. Rev. Lett.*, 105:108104, Sep 2010.
- [11] D. Wenzel and A. Voigt. Multiphase field models for collective cell migration. *Phys. Rev. E*, 104:054410, Nov 2021.
- [12] Michael Chiang, Austin Hopkins, Benjamin Loewe, M Cristina Marchetti, and Davide Marenduzzo. Intercellular friction and motility drive orientational order in cell monolayers. *Proceedings of the National Academy of Sciences*, 121(40):e2319310121, 2024.
- [13] Mattia Miotto and Lorenzo Monacelli. Entropy evaluation sheds light on ecosystem complexity. *Phys. Rev. E*, 98:042402, Oct 2018.
- [14] Austin Hopkins, Michael Chiang, Benjamin Loewe, Davide Marenduzzo, and M. Cristina Marchetti. Local yield and compliance in active cell monolayers. *Phys. Rev. Lett.*, 129:148101, Sep 2022.
- [15] Benjamin Loewe, Michael Chiang, Davide Marenduzzo, and M. Cristina Marchetti. Solid-liquid transition of deformable and overlapping active particles. *Phys. Rev. Lett.*, 125:038003, Jul 2020.
- [16] Romain Mueller, Julia M. Yeomans, and Amin Doostmohammadi. Emergence of active nematic behavior in monolayers of isotropic cells. *Phys. Rev. Lett.*, 122:048004, Feb 2019.
- [17] Fran çois Graner and James A. Glazier. Simulation of biological cell sorting using a two-dimensional extended potts model. *Phys. Rev. Lett.*, 69:2013–2016, Sep 1992.
- [18] Souvik Sadhukhan and Saroj Kumar Nandi. Theory and simulation for equilibrium glassy dynamics in cellular potts model of confluent biological tissue. *Phys. Rev. E*, 103:062403, Jun 2021.

- [19] R. Belousov, S. Savino, P. Moghe, T. Hiiragi, L. Rondoni, and A. Erzberger. Poissonian cellular potts models reveal nonequilibrium kinetics of cell sorting. *Phys. Rev. Lett.*, 132:248401, Jun 2024.
- [20] James A. Glazier and François Graner. Simulation of the differential adhesion driven rearrangement of biological cells. *Phys. Rev. E*, 47:2128–2154, Mar 1993.
- [21] Tatsuzo Nagai and Hisao Honda. A dynamic cell model for the formation of epithelial tissues. *Philosophical Magazine B*, 81(7):699–719, 2001.
- [22] Dapeng Bi, JH Lopez, Jennifer M Schwarz, and M Lisa Manning. A density-independent rigidity transition in biological tissues. *Nature Physics*, 11(12):1074–1079, 2015.
- [23] Dapeng Bi, Xingbo Yang, M. Cristina Marchetti, and M. Lisa Manning. Motility-driven glass and jamming transitions in biological tissues. *Phys. Rev. X*, 6:021011, Apr 2016.
- [24] Fabio Giavazzi, Matteo Paoluzzi, Marta Macchi, Dapeng Bi, Giorgio Scita, M Lisa Manning, Roberto Cerbino, and M Cristina Marchetti. Flocking transitions in confluent tissues. *Soft matter*, 14(18):3471–3477, 2018.
- [25] Matthias Merkel and M Lisa Manning. A geometrically controlled rigidity transition in a model for confluent 3d tissues. *New Journal of Physics*, 20(2):022002, 2018.
- [26] Matthias Merkel, Karsten Baumgarten, Brian P Tighe, and M Lisa Manning. A minimal-length approach unifies rigidity in underconstrained materials. *Proceedings of the National Academy of Sciences*, 116(14):6560–6568, 2019.
- [27] Gonca Erdemci-Tandogan and M Lisa Manning. Effect of cellular rearrangement time delays on the rheology of vertex models for confluent tissues. *PLoS computational biology*, 17(6):e1009049, 2021.
- [28] Mattia Miotto and Lorenzo Monacelli. Genome heterogeneity drives the evolution of species. *Phys. Rev. Res.*, 2:043026, Oct 2020.
- [29] Xingbo Yang, Dapeng Bi, Michael Czajkowski, Matthias Merkel, M Lisa Manning, and M Cristina Marchetti. Correlating cell shape and cellular stress in motile confluent tissues. *Proceedings of the National Academy of Sciences*, 114(48):12663–12668, 2017.
- [30] Reza Farhadifar, Jens-Christian Röper, Benoit Aigouy, Suzanne Eaton, and Frank Jülicher. The influence of cell mechanics, cell-cell interactions, and proliferation on epithelial packing. *Current biology*, 17(24):2095–2104, 2007.
- [31] Mattia Miotto, Maria Rosito, Matteo Paoluzzi, Valeria de Turreis, Viola Fölll, Marco Leonetti, Giancarlo Ruocco, Alessandro Rosa, and Giorgio Gosti. Collective behavior and self-organization in neural rosette morphogenesis. *Frontiers in Cell and Developmental Biology*, 11, August 2023.
- [32] Raimon Sunyer, Vito Conte, Jorge Escribano, Alberto Elosegui-Artola, Anna Labernadie, Léo Valon, Daniel Navajas, José Manuel García-Aznar, José J Muñoz, Pere Roca-Cusachs, et al. Collective cell durotaxis emerges from long-range intercellular force transmission. *Science*, 353(6304):1157–1161, 2016.
- [33] Peter Friedl and Roberto Mayor. Tuning collective cell migration by cell-cell junction regulation. *Cold Spring Harbor perspectives in biology*, 9 (4):a029199, 2017.
- [34] Mattia Miotto and Lorenzo Monacelli. Tolomeo, a novel machine learning algorithm to measure information and order in correlated networks and predict their state. *Entropy*, 23(9):1138, August 2021.
- [35] Jin-Ah Park, Jae Hun Kim, Dapeng Bi, Jennifer A. Mitchel, Nader Taheri Qazvini, Kelan Tantisira, Chan Young Park, Maureen McGill, Sae-Hoon Kim, Bomi Gweon, Robert Steward Jr Jacob Notbohm, Stephanie Burger, Scott H. Randell, Alvin T. Kho, Dhananjay T. Tambe, Corey Hardin, Stephanie A. Shore, Elliot Israel, David A. Weitz, Daniel J. Tschumperlin, Elizabeth P. Henske, Scott T. Weiss, M. Lisa Manning, James P. Butler, Jeffrey M. Drazen, and Jeffrey J. Fredberg. Unjamming and cell shape in the asthmatic airway epithelium. *Nature Materials*, 14:1040–1048, 2015.
- [36] Pragya Arora, Souvik Sadhukhan, Saroj Kumar Nandi, Dapeng Bi, A. K. Sood, and Rajesh Ganapathy. A shape-driven reentrant jamming transition in confluent monolayers of synthetic cell-mimics. *Nature Communications*, 15(1), July 2024.
- [37] Souvik Sadhukhan, Manoj Kumar Nandi, Satyam Pandey, Matteo Paoluzzi, Chandan Dasgupta, Nir Gov, and Saroj Kumar Nandi. How motility drives the glassy dynamics in confluent epithelial monolayers? *bioRxiv*, March 2024.
- [38] Chiara Malinverno, Salvatore Corallino, Fabio Giavazzi, Martin Bergert, Qingsen Li, Marco Leoni, Andrea Disanza, Emanuela Frittoli, Amanda Oldani, Emanuele Martini, Tobias Lendenmann, Gianluca De Florian, Galina V. Beznoussenko, Dimos Poulidakos, Kok Haur Ong, Marina Uroz, Xavier Trepas, Dario Parazzoli, Paolo Maiuri, Weimiao Yu, Aldo Ferrari, Roberto Cerbino, and Giorgio Scita. Endocytic reawakening of motility in jammed epithelia. *Nature Materials*, 16:587–596, January 2017.
- [39] Wenyang Kang, Jacopo Ferruzzi, Catalina-Paula Spatarelu, Yu Long Han, Yasha Sharma, Stephan A Koehler, Jennifer A Mitchel, Adil Khan, James P Butler, Darren Roblyer, et al. A novel jamming phase diagram links tumor invasion to non-equilibrium phase separation. *IScience*, 24(11), 2021.
- [40] Jennifer A. Mitchel, Amit Das, Michael J. O’Sullivan, Ian T. Stancil, Stephen J. DeCamp, Stephan Koehler, Oscar H. Ocaña, James P. Butler, Jeffrey J. Fredberg, M. Angela Nieto, Dapeng Bi, and Jin-Ah Park. In primary airway epithelial cells, the unjamming transition is distinct from the epithelial-to-mesenchymal transition. *Nature Communications*, 11(1), October 2020.
- [41] Nen Saito and Shuji Ishihara. Cell deformability drives fluid-to-fluid phase transition in active cell monolayers. *Science Advances*, 10(19), May 2024.
- [42] Francisco J Calero-Cuenca, Cátia S Janota, and Edgar R Gomes. Dealing with the nucleus during cell migration. *Current Opinion in Cell Biology*, 50:35–41, February 2018.
- [43] Arthur Boutillon, Samhita P. Banavar, and Otger Campàs. Conserved physical mechanisms of cell and tissue elongation. *Development*, 151(10), May 2024.
- [44] Katarina Wolf, Mariska te Lindert, Marina Krause, Stephanie Alexander, Joost te Riet, Amanda L. Willis, Robert M. Hoffman, Carl G. Figdor, Stephen J. Weiss, and Peter Friedl. Physical limits of cell migration: Control by ecm space and nuclear deformation and tuning by proteolysis and traction force. *Journal of Cell Biology*, 201(7):1069–1084, June 2013.
- [45] Steffen Grosser, Jürgen Lippoldt, Linda Oswald, Matthias Merkel, Daniel M. Sussman, Frédéric Renner, Pablo Gottheil, Erik W. Morawetz, Thomas Fuhs, Xiaofan Xie, Steve Pawlizak, Anatol W. Fritsch, Benjamin

- Wolf, Lars-Christian Horn, Susanne Briest, Bahriye Aktas, M. Lisa Manning, and Josef A. Käs. Cell and nucleus shape as an indicator of tissue fluidity in carcinoma. *Physical Review X*, 11(1), February 2021.
- [46] Robert Chojowski, Ulrich S. Schwarz, and Falko Ziebert. The role of the nucleus for cell mechanics: an elastic phase field approach. *Soft Matter*, 20(22):4488–4503, 2024.
- [47] J. Tailleur and M. E. Cates. Statistical mechanics of interacting run-and-tumble bacteria. *Phys. Rev. Lett.*, 100:218103, May 2008.
- [48] Pasquale Digregorio, Demian Levis, Antonio Suma, Leticia F Cugliandolo, Giuseppe Gonnella, and Ignacio Pagonabarraga. Full phase diagram of active brownian disks: from melting to motility-induced phase separation. *Physical review letters*, 121(9):098003, 2018.
- [49] Vanni Petrolli, Magali Le Goff, Monika Tadrous, Kirsten Martens, Cédric Allier, Ondrej Mandula, Lionel Hervé, Silke Henkes, Rastko Sknepnek, Thomas Boudou, et al. Confinement-induced transition between wavelike collective cell migration modes. *Physical review letters*, 122(16):168101, 2019.